RESEARCH ARTICLE | JANUARY 15 2025

Enhanced tunnel magnetoresistance of Fe/$MgGa_2O_4$/Fe(001) magnetic tunnel junctions by interface-tuning with atomic-scale MgO insertion layers

Rombang Rizky Sihombing ; Thomas Scheike ; Jun Uzuhashi ; Tadakatsu Ohkubo ; Zhenchao Wen ; Seiji Mitani ; Hiroaki Sukegawa

Appl. Phys. Lett. 126, 022407 (2025)
https://doi.org/10.1063/5.0247660

Enhanced tunnel magnetoresistance of Fe/$MgGa_2O_4$/Fe(001) magnetic tunnel junctions by interface-tuning with atomic-scale MgO insertion layers

Cite as: Appl. Phys. Lett. **126**, 022407 (2025); doi: 10.1063/5.0247660
Submitted: 7 November 2024 · Accepted: 1 January 2025 ·
Published Online: 15 January 2025

View Online Export Citation CrossMark

Rombang Rizky Sihombing,[1,2] Thomas Scheike,[1] Jun Uzuhashi,[1] Tadakatsu Ohkubo,[1] Zhenchao Wen,[1] Seiji Mitani,[1,2] and Hiroaki Sukegawa[1,a)]

AFFILIATIONS

[1]National Institute for Materials Science (NIMS), 1-2-1 Sengen, Tsukuba 305-0047, Japan
[2]Graduate School of Science and Technology, University of Tsukuba, Tsukuba 305-8577, Japan

[a)]Author to whom correspondence should be addressed: sukegawa.hiroaki@nims.go.jp

ABSTRACT

We demonstrate a significant effect of atomic-scale MgO insertion layers on the tunnel magnetoresistance (TMR) in epitaxial magnetic tunnel junctions (MTJs) using a small bandgap oxide $MgGa_2O_4$. An enhanced TMR ratio of 151% at room temperature (resistance area product, *RA*: 23 kΩ · μm^2) and 291% at 5 K (*RA*: 26 kΩ · μm^2) were observed using 0.3 nm MgO insertion layers at the bottom and top barrier interfaces in Fe/$MgGa_2O_4$/Fe(001) MTJs with a total barrier thickness of 2.3 nm. The TMR showed a strong MgO thickness dependence. Microstructure analyses revealed that after MgO insertion, a homogeneous rock-salt structured $Mg_{0.55}Ga_{0.45}O$(001) barrier is formed, which differs from the nominal spinel crystal $MgGa_2O_4$. Elemental mapping of the MTJ showed that Ga diffusion into the adjacent Fe can be effectively suppressed while maintaining perfect lattice-matching at the Fe/barrier interfaces, thereby improving effective tunneling spin polarization through the barrier. The *RA* of the $Mg_{0.55}Ga_{0.45}O$ (2.3 nm) MTJ is smaller than that of a comparable $MgAl_2O_4$ barrier (2.3 nm), thanks to the lower barrier height of the $Mg_{0.55}Ga_{0.45}O$ as confirmed by the current–voltage characteristics.

Magnetic tunnel junctions (MTJs), consisting of a ferromagnetic layer (FM)/ultra-thin insulator (barrier)/FM structure, are widely used in spintronic applications, including read heads of hard disk drives (HDDs) and magnetoresistive random access memory (MRAM) cells.[1] Recently, new MTJ applications, such as ultra-highly sensitive magnetic sensors and neuromorphic devices, have also attracted much attention.[2–6] Most practical MTJs use insulating MgO as a barrier layer.[7–10] However, state-of-the-art spin-transfer-torque (STT)-MRAMs and HDD heads require very low resistance area product (*RA*) less than a few Ω · μm^2 by reducing the MgO thickness to about 1 nm (∼5 monolayers) or less.[11] Ultra-thin barriers are sensitive to imperfections with small error margins with respect to their crystallinity and flatness, leading to reduced reliability and increased risk of failure of the MTJ when, i.e., a moderate bias voltage is applied. By using new barrier materials with a lower barrier height, the thickness of the barrier can be increased while keeping *RA* low.

A magnesium gallium spinel oxide, $MgGa_2O_4$ (MGO), is a promising MTJ barrier due to its bandgap of ∼4.7 eV, which is much smaller than that of typical barriers, such as MgO and $MgAl_2O_4$ (∼8 eV).[12,13] Sukegawa *et al.*[14] reported a relatively large tunnel magnetoresistance (TMR) ratio of 121% in an epitaxial Fe/MGO/Fe MTJ at room temperature (RT). It was also shown that the *RA* of the Fe/MGO/Fe MTJ was significantly lower than that of an Fe/$MgAl_2O_4$/Fe MTJ with the same barrier thickness. First-principles calculations predicted that MGO-based MTJs exhibit a large TMR ratio and low *RA*,[15] making the MGO barrier a good option to be developed for future MTJ devices.

One of the issues with MGO-based MTJs is that achieving a larger TMR ratio at RT is necessary for practical applications. Fine-tuning of the barrier interface, such as nano-layer insertions and additional oxidation processes, would be promising for improving the TMR ratio in MGO-based MTJs.[16,17] Mertens *et al.*[18] reported that the insertion of ultra-thin

MgO layers at the bottom and top-MGO interfaces of CoFeB/MGO/CoFeB polycrystalline MTJs, i.e., CoFeB/MgO/MGO/MgO/CoFeB, significantly improves the perpendicular magnetic anisotropy of the CoFeB layers due to the improved interface composition. It is suggested that Ga diffusion is a major problem for MGO-based MTJs, and how to control it is key to obtain larger TMR ratios.

In this study, we fabricated epitaxial Fe/MGO/Fe(001) MTJ stacks and investigated the MgO insertion effect on magnetotransport properties at the MGO barrier interface. A strong dependence of TMR on the MgO insertion layer thickness was found for the MTJs. The optimum MgO thickness of 0.3 nm for both the bottom and top interfaces resulted in a significant enhancement in the TMR ratio, up to 151% at RT and 297% at 5 K. Second, microstructural analysis revealed that instead of a spinel structure, the MGO barrier formed a rock-salt crystal. Additionally, atomic-scale MgO insertion effectively suppresses Ga atomic diffusion at the barrier interfaces, maintaining the MGO barrier's high tunneling spin polarization as well as the low barrier height properties.

MTJ stacks were deposited on MgO(001) single crystal substrates using an ultra-high-vacuum multi-chamber magnetron sputtering system (EIKO Corp.) with a base pressure of $\sim 5 \times 10^{-7}$ Pa. The typical stack structure is MgO(001) substrate//Cr (60)/Fe (50)/bottom-MgO ($t_{\text{bot-MgO}} = 0$–1.0)/$MgGa_2O_4$ (MGO) (1.7)/top-MgO ($t_{\text{top-MgO}} = 0$ or 0.3)/Fe (5)/$Ir_{20}Mn_{80}$ (IrMn) (8)/Ru (10) [numbers in parentheses in nm, see Fig. 1(a)]. The MgO substrate was annealed *in situ* at 700 °C to remove surface contamination prior to deposition. All metallic layers were deposited using DC sputtering at RT followed by *in situ* post-annealing to improve the flatness and crystallinity of each layer. MGO and MgO were deposited from a 76.2 mm diameter $MgGa_2O_4$ and MgO sintered targets by RF sputtering using an input power of 100 W and an Ar pressure of 2.75 and 1.00 Pa, respectively. The MGO layer was post-annealed at 400 °C, followed by 300 s of natural oxidation using pure O_2 gas (99.999%, ~1 Pa) after cooling down to RT to tune the oxidation state at the top barrier interface. The bottom-MgO layer thickness was varied during deposition using a linear motion shutter. The MgO insertion layers were *in situ* post-annealed at 250 °C. High energy electron diffraction (RHEED) was used to evaluate the surface crystal structure of each layer. The MTJ stacks were annealed *ex situ* in a magnetic field of 2 kOe at 200 °C along the Fe easy axis direction, i.e., MgO[110] || Fe[100], and patterned into 4×4–8×8 μm^2 square MTJs using laser and photolithography, and Ar ion milling. Magnetotransport properties of the patterned MTJs were characterized using a conventional DC 4-probe method at RT (Keithley 2400 sourcemeter and Keithley 2182 A nanovoltmeter). The TMR ratios were measured with a bias voltage of ~10 mV. The TMR ratio (%) is defined as $100 \times (R_{AP} - R_P)/R_P$, where R_{AP} [R_P] is the resistance in the antiparallel (AP) [parallel (P)] magnetization configuration. The temperature dependence of the TMR ratio and *RA* from RT to 5 K was characterized using physical property measurement system (PPMS, Quantum Design, Dynacool). High-resolution annular dark-field scanning transmission electron microscopy (ADF-STEM), nanobeam electron diffraction (NBED), and energy dispersive x-ray spectroscopy (EDS) (Titan G2 80-200 TEM) were used to investigate the microstructure of the MTJ cross section.

The RHEED patterns at each growth stage for the epitaxial Fe/MGO/Fe with MgO insertion layers are shown in Fig. 1(b) for the MgO[100] azimuth and Fig. 1(c) for the MgO[110] azimuth, respectively. Figure 1(d) schematically shows the crystal structures and orientations reconstructed from the RHEED patterns. The pattern of the

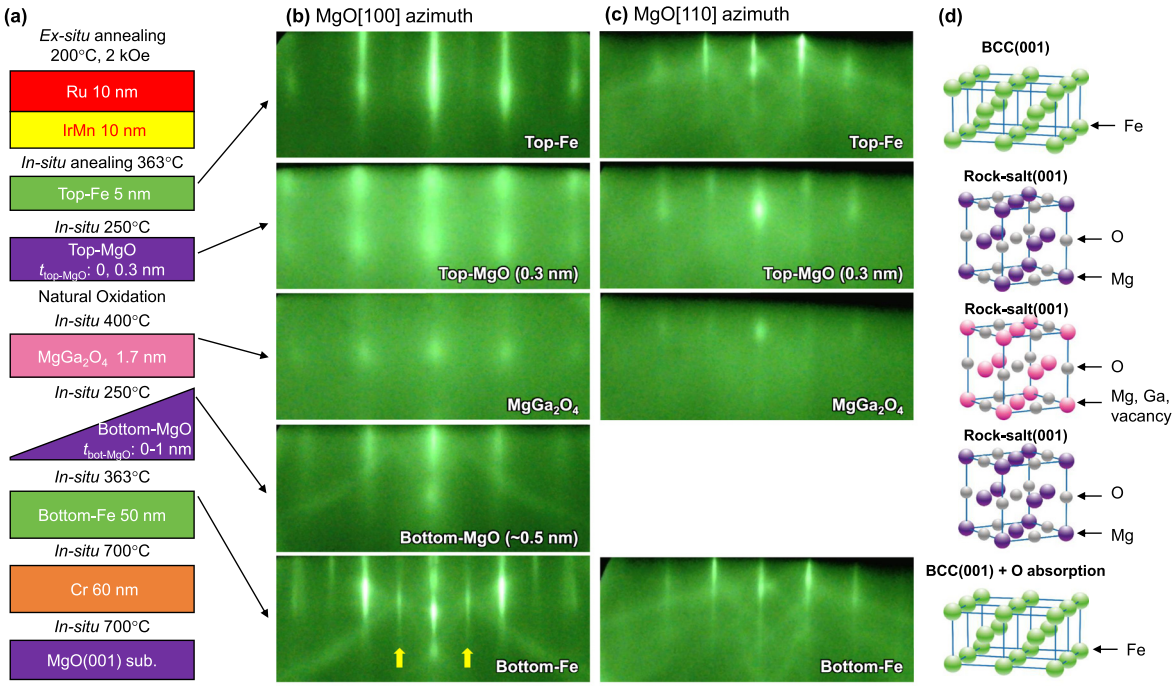

FIG. 1. (a) Schematic illustration of MTJ stacks. (b) and (c) RHEED patterns at each deposition stage for (b) MgO[100] azimuth and (c) MgO[110] azimuth. (d) Corresponding atomic structure models.

bottom Fe shows sharp streaks, indicating highly (001)-oriented bcc epitaxial growth and a flat surface. Weaker streaks marked by yellow arrows were also observed, suggesting a $c(2 \times 2)$ reconstructed surface due to oxygen adsorption during the *in situ* annealing.[19] Nevertheless, the bottom ($t_{\text{bot-MgO}} \sim 0.5$ nm) and top-MgO insertion layer exhibits epitaxial growth with a (001)-oriented rock-salt (RS) structure with 45° in-plane lattice rotation on the bottom Fe, as shown in Fig. 1(d). The MGO layer on the lower MgO also shows epitaxial growth, although it has a lower RHEED intensity than that of the lower MgO layer. The MGO also has an RS-like structure (cation-disordered spinel)[20,21] as indicated by the absence of superlattice streaks resulting in half the unit cell size of an ordered spinel MGO. The top Fe layer shows bcc (001) epitaxial growth. Thus, all layers are epitaxially grown with (001) orientation.

Figure 2(a) shows the $t_{\text{bot-MgO}}$ dependence of the TMR ratio and *RA* at RT of the MTJs with [without] the top-MgO ($t_{\text{top-MgO}} = 0.3$ nm) [($t_{\text{top-MgO}} = 0$ nm)]. In both cases, the TMR ratio increases rapidly with $t_{\text{bot-MgO}}$, reaching a maximum between 0.3 and 0.4 nm followed by a decrease for larger $t_{\text{bot-MgO}}$. The maximum TMR ratio of the MTJ with (without) top-MgO insertion reaches 151% (102%) at $t_{\text{bot-MgO}} = 0.3$ nm (0.4 nm). The MgO insertion layers can effectively increase

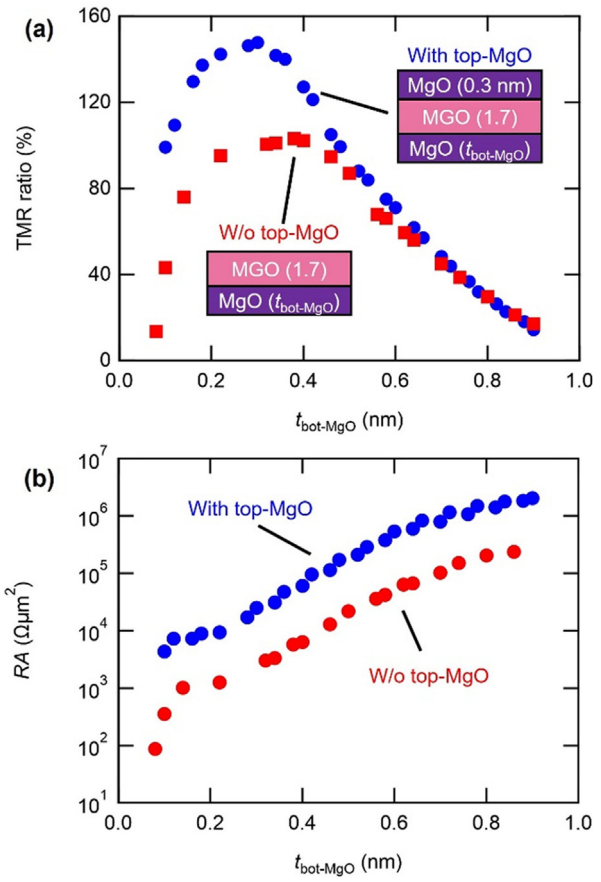

FIG. 2. $t_{\text{bot-MgO}}$ dependences of (a) TMR ratio and (b) *RA* at RT for MTJs with bottom-MgO ($t_{\text{bot-MgO}}$)/MGO/top-MgO (0.3 nm) barrier (blue symbols) and bottom-MgO ($t_{\text{bot-MgO}}$)/MGO barrier (red symbols).

the maximum TMR ratio. In the previous report of Fe/MGO/Fe MTJs,[14] a 0.6 nm Mg insertion at the bottom side of the MGO barrier increased the TMR ratio: 121% (85%) with (without) the insertion. Similarly, the MgO insertion may improve the MGO interface quality in this study. The value of 0.3 nm corresponds to 1.5 monolayers of an MgO(001) lattice; thus, this thickness may be sufficient to completely cover the Fe interfaces with MgO to block the Ga diffusion, as shown later in the nanostructural analysis. The decrease in TMR ratio observed at larger $t_{\text{bot-MgO}}$ may be due to the increase in effective in-plane lattice mismatch between the barrier and the Fe electrodes; the mismatch between MgO(001) and Fe(001) (−3.8%) is larger than that between MGO(001) and Fe(001) (−2.2%) for bulk.[13] As seen in Fig. 2(b), the log(*RA*) increases linearly with $t_{\text{bot-MgO}}$ around the large TMR regions, i.e., $t_{\text{bot-MgO}} \sim 0.25$–0.55 nm. In this thickness range, a 0.3 nm increase in $t_{\text{bot-MgO}}$ results in an almost tenfold increase in *RA*. This increase is almost the same as the increase due to the 0.3 nm top-MgO insertion. This means that the barrier thickness increases linearly with $t_{\text{bot-MgO}}$ and $t_{\text{top-MgO}}$ for both the structures. Therefore, both the MgO/MGO and MgO/MGO/MgO barriers work as a single layer tunnel barrier for MTJs.

Figures 3(a) and 3(b) show the TMR ratio and *RA* as a function of the in-plane magnetic field of the Fe/MgO ($t_{\text{bot-MgO}} = 0.3$ nm)/MGO/MgO ($t_{\text{top-MgO}} = 0.3$ nm)/Fe at RT and 5 K, respectively. A maximum TMR ratio of 151% and an *RA* of 23 kΩ · μm² at RT were observed with clear magnetic switching. At 5 K, the TMR ratio almost doubles to 291% (*RA*: 26 kΩ · μm²), demonstrating a significant spin-dependent coherent tunneling through the MgO/MGO/MgO barrier. These TMR ratios are much larger than those reported values in a Fe/Mg (0.6 nm)/MGO/Fe MTJ (121% at RT and 165% at low temperatures).[14] The effective tunneling spin polarization P_{eff} at 5 K is calculated to be 0.77 based on the Julliere formula, TMR ratio $= 100 \times 2P_{\text{eff}}^2/(1 - P_{\text{eff}}^2)$, assuming P_{eff} is the same for both interfaces.[22] Figures 3(c) and 3(d) show the temperature dependences of the *RA* for the P (RA_{P}) and AP (RA_{AP}) states, and the TMR ratio of the MTJ, respectively. The RA_{AP} decreases significantly with increasing temperature, while the RA_{P} is almost constant. Therefore, the RA_{AP} primarily determines the temperature dependence of the TMR ratio. This behavior can be attributed to the occurrence of spin-dependent coherent tunneling though the Δ_1 state for the P state, as observed in MgO-based and $MgAl_2O_4$-based MTJs with large TMR ratios.[16,23–25]

Figures 4(a) and 4(b) show the cross-sectional ADF-STEM images of Fe/MgO (0.3 nm)/MGO (1.6 nm) MgO (0.3 nm)/Fe with *RA* of 16.5 kΩ · μm². The image shows the formation of high-quality epitaxial Fe/MgO/MGO/MgO/Fe with atomically flat interfaces for both the bottom-Fe/MgO/MGO and MGO/MgO/top-Fe sides. Only a few misfit dislocations were observed at the interfaces, indicating nearly perfect lattice-matching between Fe and the barrier. The NBED patterns taken from the bottom Fe and top Fe electrodes show their good crystallinity with bcc(001) orientation, as expected from the RHEED patterns shown in Figs. 1(b) and 1(c). The pattern of the MgO/MGO/MgO barrier [Fig. 4(d)] shows an RS(001) structure, consistent with the RHEED patterns of the MGO layer. The EDS elemental maps of Mg, Ga, O, and Fe shown in Figs. 4(f)–4(j) indicate that the element distribution in the barrier is homogeneous. The barrier composition was determined to be $(Mg_{0.55}Ga_{0.45})_{0.47}O_{0.53}$ (hereafter, $Mg_{0.55}Ga_{0.45}O$) using Gaussian fits of Mg, Ga, and O as shown in the supplementary material, Fig. S1. Therefore, the formation of the RS structure is mainly

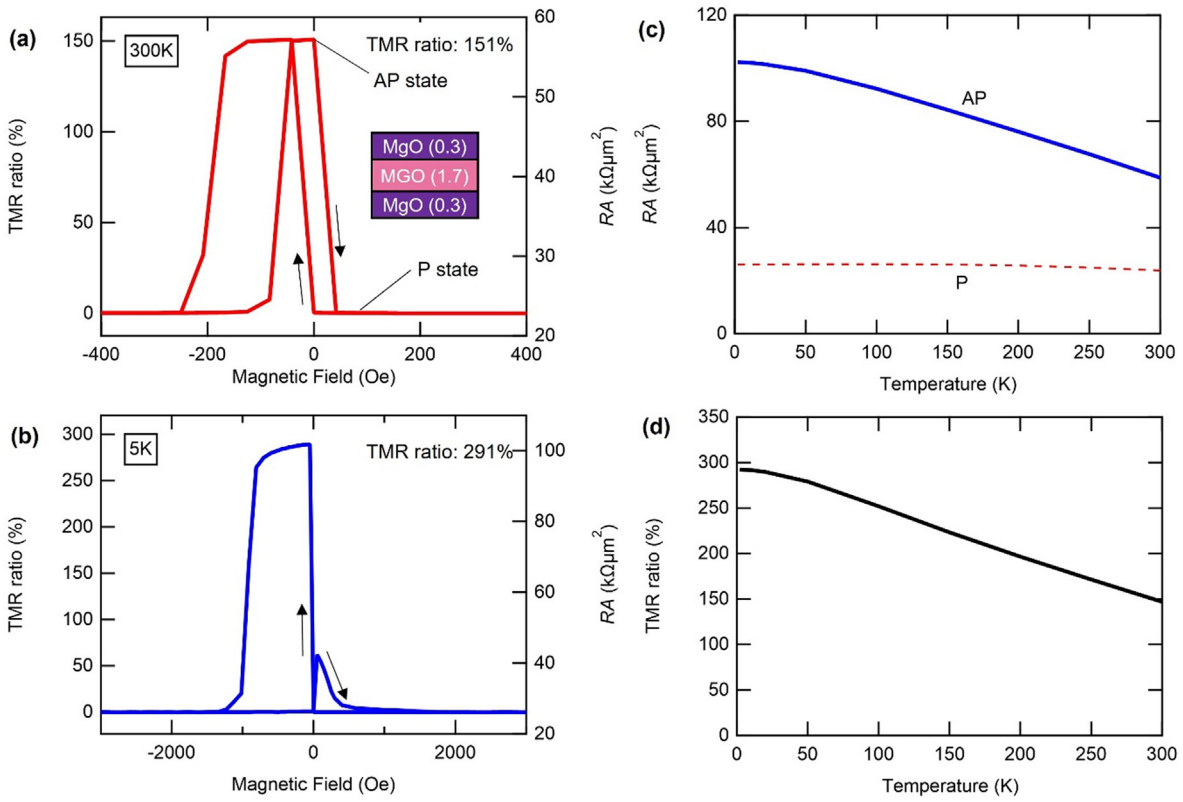

FIG. 3. (a) and (b) TMR ratio and *RA* as a function of magnetic field of Fe/MgO (0.3)/MGO (1.7)/MgO (0.3 nm)/Fe MTJ measured at (a) RT and (b) 5 K. (c) and (d) Temperature dependences of (c) *RA* for P and AP states and (d) TMR ratio.

due to the off-stoichiometric MGO composition by mixing of Mg and Ga atoms in the MgO/MGO/MgO trilayer. The EDS line profiles shown in Fig. 4(k) indicate that there is no significant interdiffusion of Ga atoms into the bottom- and top-Fe side. This means that MgO insertion layers with optimum thickness of 0.3 nm act as good Ga diffusion barriers to make both the Fe interfaces chemically sharp, resulting in TMR enhancements. In $MgAl_2O_4$(001)-based MTJs, the cation site disorder that halves the unit cell size, i.e., the change from a spinel structure (a_{spinel}) to an RS-like structure ($a_{RS} \sim a_{spinel}/2$), can effectively improve the TMR ratios due to suppression of the band-folding effect.[20,26] Therefore, the formation of RS-like MGO barrier may also be one of the possible origins of the improved TMR ratios. The estimated barrier thickness was ~2.3 nm, which is close to the design structure of the MgO/MGO/MgO (=2.2 nm). The *RA* of 16.5 $k\Omega \cdot \mu m^2$ of the Fe/$Mg_{0.55}Ga_{0.45}O$ (2.3 nm)/Fe is 8 times higher than that of Fe/$MgGa_2O_4$ (2.3 nm)/Fe, but it is still 3 times lower than that of Fe/$MgAl_2O_4$ (2.3 nm)/Fe.[14] Therefore, *RA* reduction is observed even after the 0.6 nm MgO insertion.

We evaluated the current–voltage (*I*–*V*) curves and bias voltage dependence of the TMR ratio of the Fe/MgO (0.3 nm)/MGO (1.7 nm)/MgO (0.3 nm)/Fe MTJ at RT, and 5 K. Figures 5(a) and 5(d) show *I*–*V* curves and Figs. 5(b) and 5(e) show the *dI*/*dV* curves at RT (5 K), respectively. Positive bias is defined as the direction in which electrons tunnel from the top electrode to the bottom electrode, as shown in the inset of (a). The *dI*/*dV* curves are obtained by numerical differentiation of the *I*–*V* curves. In both the P and AP states, |*I*| and *dI*/*dV* curves increase significantly when the bias voltage exceeds |0.5 V| for both bias polarities. In MgO- and $MgAl_2O_4$-based MTJs, such a significant current acceleration is typically not observed below |1 V|. In MgO- and $MgAl_2O_4$-based MTJs with large TMR ratios, significantly large local minima can be observed in the *dI*/*dV* curves in the P state.[16,17,23] However, our MGO-MTJ does not clearly show such structures in the *dI*/*dV* curves even at 5 K.

We fitted the *I*–*V* curves using the Simmons equation to estimate the effective barrier height of the $Mg_{0.55}Ga_{0.45}O$.[27] The fitting results are shown in Table I, in addition to the values in the previous reports.[14] Typical log(*I*)–log(*V*) plots with fitting curves of the Simmons equation are shown in the supplementary material, Fig. S2. The experimental data were well fitted by the equation for both positive and negative bias. For the positive bias, the effective barrier height (ϕ_{eff}) was 0.86 eV in the P state and 0.70 eV in the AP state at 300 K. For the negative bias, ϕ_{eff} was 1.1 eV in the P state and 0.82 eV in the AP state at 300 K. These values are comparable to the barrier height of the previous Fe/$MgGa_2O_4$/Fe MTJ and much smaller than that of the Fe/$MgAl_2O_4$/Fe MTJ.[14] We also found a large temperature dependence in the barrier height of Fe/$Mg_{0.55}Ga_{0.45}O$/Fe [see Figs. S2(b) and S2(d)], indicating the low barrier feature.[27] The low barrier height is maintained even after the insertion of MgO.

Figures 5(c) and 5(f) show the bias voltage dependences of the normalized TMR ratio by its zero bias value of the Fe/MgO (0.3 nm)/

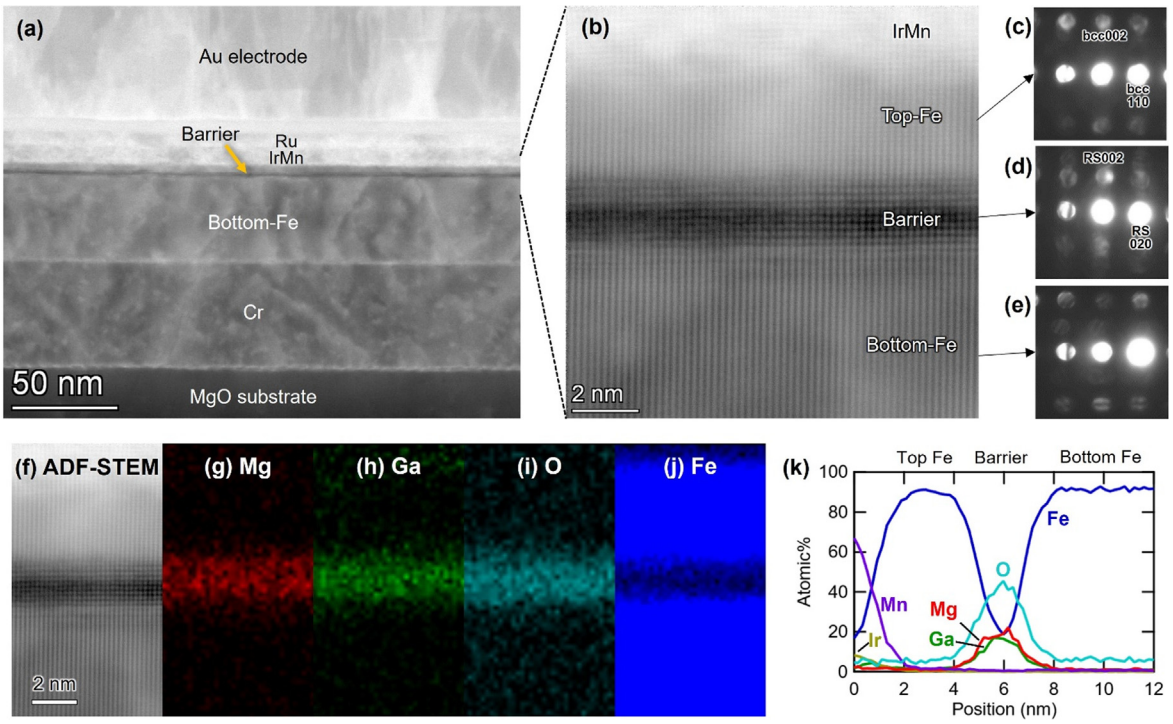

FIG. 4. (a) Low magnification and (b) high magnification ADF-STEM images of Fe/MgO (0.3)/MGO (1.6)/MgO (0.3 nm)/Fe MTJ. (c)–(e) NBED patterns taken from (c) top Fe, (d) barrier, and (e) bottom Fe. (f)–(j) EDS maps for (f) ADF image, (g) Mg, (h) Ga, (i) O, and (j) Fe. (k) Corresponding EDS profiles.

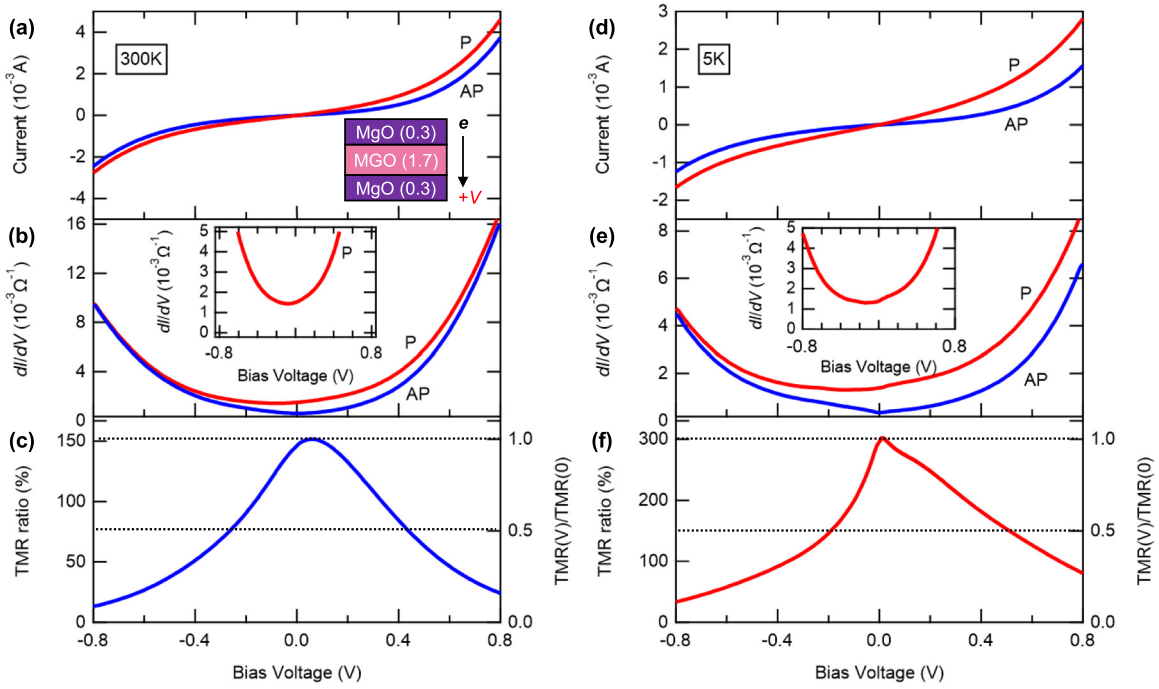

FIG. 5. (a) and (d) *I*–*V* curves, (b) and (e) *dI*/*dV* curves, (c) and (f) bias voltage dependence of normalized TMR of Fe/MgO (0.3)/MGO (1.7)/MgO (0.3 nm)/Fe MTJ (device area: 8 × 8 μm^2) for RT and 5 K, respectively. The insets of (b) and (e) are close-ups of the *dI*/*dV* curves for the P state.

TABLE I. Summary of Simmons fit results for Fe/barrier/Fe(001) MTJs for the positive bias direction.

Barrier structure (Unit: nm)	State	t_{eff} (nm)	ϕ_{eff} (eV)
MgO (0.3)/$MgGa_2O_4$ (1.7)/ MgO (0.3) (present study)	P	1.42	0.86
	AP	1.65	0.70
$MgGa_2O_4$ (2.4) (Ref. 14)	P	0.96	0.96
	AP	1.1	1.0
$MgAl_2O_4$ (2.4) (Ref. 14)	P	0.89	3.0
	AP	1.1	2.1

MGO (1.7 nm)/MgO (0.3 nm)/Fe MTJ at RT and 5 K, respectively. The asymmetry of the TMR ratio with the bias polarity is larger than that of the *I*–*V* characteristics. Due to the low barrier height, a larger bias voltage dependence of the TMR ratio is expected: V_{half}, the bias voltage where the TMR becomes half the value of zero bias, is 0.43 V (−0.26 V) for the positive (negative) bias at RT, which is less than half the values in Fe/$MgAl_2O_4$/Fe MTJs.[24,25] At 5 K, the asymmetric feature is more pronounced. Note that the asymmetry in the *I*–*V* characteristics and the differences in barrier height and V_{half} between the positive and negative bias are attributed to the slight difference in interface states between the top and bottom $Mg_{0.55}Ga_{0.45}O$ interfaces, which cannot be detected by the present STEM analysis. Therefore, further improvement of the bottom and top interfaces can significantly improve the TMR ratio of MGO-based MTJs.

In summary, we investigated the effect of MgO insertion layers on magnetotransport properties using epitaxial Fe/MGO/Fe(001). Nanostructural analysis revealed the formation of a uniform barrier layer with an RS structure with a $Mg_{0.55}Ga_{0.45}O$ composition. The MgO layers effectively suppress Ga interdiffusion into the top and bottom Fe layers, resulting in the formation of a lattice-matched Fe/$Mg_{0.55}Ga_{0.45}O$/Fe(001) MTJ. The interfacial modification by MgO insertions significantly improves the TMR ratio up to 151% at RT (291% at 5 K) while maintaining the low barrier height. Our results indicate that an MGO-based barrier is promising as a low *RA* barrier with significant coherent tunneling effect, which can be beneficial for next generation spintronic applications such as ultra-high density MRAMs.

See the supplementary material for the EDS Gaussian fit results for the barrier and the Simmons fits for the log(*I*)–log(*V*) characteristics.

The authors thank Hiromi Ikeda and Chika Shigaki for their technical support on device microfabrication. This work was partially supported by KIOXIA Corporation, MEXT Program: Data Creation and Utilization-Type Material Research and Development Project (Grant No. JPMXP1122715503) and JSPS KAKENHI (Grant Nos. 21H01750, 22H04966, and 24H00408). R.R.S. thanks the National Institute for Materials Science for the provision of a NIMS Junior Research Assistantship.

AUTHOR DECLARATIONS

Conflict of Interest

The authors have no conflicts to disclose.

Author Contributions

Rombang Rizky Sihombing: Data curation (lead); Formal analysis (equal); Investigation (lead); Methodology (equal); Visualization (lead); Writing – original draft (equal); Writing – review & editing (equal). **Thomas Scheike:** Methodology (supporting); Validation (equal); Writing – review & editing (equal). **Jun Uzuhashi:** Data curation (equal); Investigation (equal); Validation (equal); Visualization (equal); Writing – review & editing (supporting). **Tadakatsu Ohkubo:** Investigation (equal); Validation (equal); Writing – review & editing (supporting). **Zhenchao Wen:** Investigation (supporting); Methodology (supporting); Writing – review & editing (supporting). **Seiji Mitani:** Funding acquisition (equal); Methodology (supporting); Supervision (equal); Validation (lead); Writing – original draft (supporting); Writing – review & editing (lead). **Hiroaki Sukegawa:** Conceptualization (lead); Formal analysis (equal); Funding acquisition (lead); Investigation (equal); Methodology (equal); Supervision (lead); Visualization (equal); Writing – original draft (lead); Writing – review & editing (equal).

DATA AVAILABILITY

The data that support the findings of this study are available within the article and from the corresponding author upon reasonable request.

REFERENCES

[1]S. Yuasa and D. D. Djayaprawira, J. Phys. Appl. Phys. **40**, R337 (2007).
[2]P. P. Freitas, R. Ferreira, and S. Cardoso, Proc. IEEE **104**, 1894 (2016).
[3]J. Torrejon, M. Riou, F. A. Araujo, S. Tsunegi, G. Khalsa, D. Querlioz, P. Bortolotti, V. Cros, K. Yakushiji, A. Fukushima, H. Kubota, S. Yuasa, M. D. Stiles, and J. Grollier, Nature **547**, 428 (2017).
[4]N. Maciel, E. Marques, L. Naviner, Y. Zhou, and H. Cai, Sensors **20**, 121 (2019).
[5]A. Fukushima, T. Yamamoto, T. Nozaki, K. Yakushiji, H. Kubota, and S. Yuasa, APL Mater. **9**, 030905 (2021).
[6]S. Jung, H. Lee, S. Myung, H. Kim, S. K. Yoon, S. W. Kwon, Y. Ju, M. Kim, W. Yi, S. Han, B. Kwon, B. Seo, K. Lee, G. H. Koh, K. Lee, Y. Song, C. Choi, D. Ham, and S. J. Kim, Nature **601**, 211 (2022).
[7]W. Butler, X.-G. Zhang, T. Schulthess, and J. MacLaren, Phys. Rev. B **63**, 054416 (2001).
[8]J. Mathon and A. Umerski, Phys. Rev. B **63**, 220403 (2001).
[9]S. S. P. Parkin, C. Kaiser, A. Panchula, P. M. Rice, B. Hughes, M. Samant, and S.-H. Yang, Nat. Mater. **3**, 862 (2004).
[10]S. Yuasa, T. Nagahama, A. Fukushima, Y. Suzuki, and K. Ando, Nat. Mater. **3**, 868 (2004).
[11]G. Albuquerque, S. Hernandez, M. T. Kief, D. Mauri, and L. Wang, IEEE Trans. Magn. **58**, 1 (2022).
[12]Z. Galazka, D. Klimm, K. Irmscher, R. Uecker, M. Pietsch, R. Bertram, M. Naumann, M. Albrecht, A. Kwasniewski, R. Schewski, and M. Bickermann, Phys. Status Solidi A **212**, 1455 (2015).
[13]M. Coll, J. Fontcuberta, M. Althammer, M. Bibes, H. Boschker, A. Calleja, G. Cheng, M. Cuoco, R. Dittmann, B. Dkhil, I. E. Baggari, M. Fanciulli, I. Fina, E. Fortunato, C. Frontera, S. Fujita, V. Garcia, S. T. B. Goennenwein, C. G. Granqvist, J. Grollier, R. Gross, A. Hagfeldt, G. Herranz, K. Hono, E. Houwman, M. Huijben, A. Kalaboukhov, D. J. Keeble, G. Koster, L. F. Kourkoutis, J. Levy, M. Lira-Cantu, J. L. MacManus-Driscoll, J. Mannhart, R. Martins, S. Menzel, T. Mikolajick, M. Napari, M. D. Nguyen, G. Niklasson, C. Paillard, S. Panigrahi, G. Rijnders, F. Sánchez, P. Sanchis, S. Sanna, D. G. Schlom, U. Schroeder, K. M. Shen, A. Siemon, M. Spreitzer, H. Sukegawa, R. Tamayo, J. van den Brink, N. Pryds, and F. M. Granozio, Appl. Surf. Sci. **482**, 1 (2019).
[14]H. Sukegawa, Y. Kato, M. Belmoubarik, P. H. Cheng, T. Daibou, N. Shimomura, Y. Kamiguchi, J. Ito, H. Yoda, T. Ohkubo, S. Mitani, and K. Hono, Appl. Phys. Lett. **110**, 122404 (2017).
[15]K. Nawa, K. Masuda, and Y. Miura, Phys. Rev. B **102**, 144423 (2020).

[16]T. Scheike, Q. Xiang, Z. Wen, H. Sukegawa, T. Ohkubo, K. Hono, and S. Mitani, Appl. Phys. Lett. **118**, 042411 (2021).
[17]T. Scheike, Z. Wen, H. Sukegawa, and S. Mitani, Appl. Phys. Lett. **122**, 112404 (2023).
[18]S. Mertens, S. Couet, R. Carpenter, J. Swerts, D. Crotti, and G. S. Kar, Appl. Phys. Lett. **118**, 172402 (2021).
[19]J. W. Koo, S. Mitani, T. T. Sasaki, H. Sukegawa, Z. C. Wen, T. Ohkubo, T. Niizeki, K. Inomata, and K. Hono, Appl. Phys. Lett. **103**, 192401 (2013).
[20]H. Sukegawa, Y. Miura, S. Muramoto, S. Mitani, T. Niizeki, T. Ohkubo, K. Abe, M. Shirai, K. Inomata, and K. Hono, Phys. Rev. B **86**, 184401 (2012).
[21]J. P. Hadorn, H. Sukegawa, T. Ohkubo, S. Mitani, and K. Hono, Acta Mater. **145**, 306–315 (2018).
[22]M. Julliere, Phys. Lett. A **54**, 225 (1975).
[23]V. Drewello, J. Schmalhorst, A. Thomas, and G. Reiss, Phys. Rev. B **77**, 014440 (2008).
[24]H. Sukegawa, H. Xiu, T. Ohkubo, T. Furubayashi, T. Niizeki, W. Wang, S. Kasai, S. Mitani, K. Inomata, and K. Hono, Appl. Phys. Lett. **96**, 212505 (2010).
[25]M. Belmoubarik, H. Sukegawa, T. Ohkubo, S. Mitani, and K. Hono, Appl. Phys. Lett. **108**, 132404 (2016).
[26]Y. Miura, S. Muramoto, K. Abe, and M. Shirai, Phys. Rev. B **86**, 024426 (2012).
[27]J. G. Simmons, J. Appl. Phys. **34**, 1793 (1963).